Advanced Microstructural Study of Suspension Plasma Sprayed Hydroxyapatite Coatings

Harry Podlesak, Lech Pawlowski, Romain d'Haese, Jacky Laureyns, Thomas Lampke, and Severine Bellayer

Fine, home-synthesized, hydroxyapatite powder was formulated with water and alcohol to obtain a suspension used to plasma spray coatings onto a titanium substrate. The deposition process was optimized using statistical design of 2^n experiments with two variables: spray distance and electric power input to plasma. X-ray diffraction (XRD) was used to determine quantitatively the phase composition of obtained deposits. Raman microscopy and electron probe microanalysis (EPMA) enabled localization of the phases in different positions of the coating cross sections. Transmission electron microscopic (TEM) study associated with energy-dispersive x-ray spectroscopy (EDS) enabled visualization and analysis of a two-zone microstructure. One zone contained crystals of hydroxyapatite, tetracalcium phosphate, and a phase rich in calcium oxide. This zone included lamellas, usually observed in thermally sprayed coatings. The other zone contained fine hydroxyapatite grains that correspond to nanometric and submicrometric solids from the suspension that were agglomerated and sintered in the cold regions of plasma jet and on the substrate.

1. Introduction

Biomaterials interact with biological systems, in particular, in prostheses of hips, knees, and so forth. Hydroxyapatite (HA), $Ca_5(PO_4)_3OH$, has been used since 1990 as a coating on the prostheses to enhance its biointegration with bone. The coatings are deposited mainly by plasma spraying (Ref 1). For the typical price of hip prosthesis of about 700 €, the total cost of surface engineering including coating deposition is about 50 €. Taking into account that the total number of hips and knees implants is about 1 million/year and that high-quality hydroxyapatite powder costs about 300 €/kg, the development of new coating technologies should consider the reduction of cost. One such technology is suspension plasma spraying, which can reduce the thickness of coatings down to 10 to 50 μm. The technology of suspension plasma spraying hydroxyapatite coatings was initiated in the mid-1990s at The University of Sherbrooke in Canada

(Ref 2, 3). The technology is based on injection of fine nanometric or submicronic powder particles suspension into high-temperature plasma. The slurry dries up, and the fine particles are sintered in plasma and become molten before striking the substrate (Ref 4). The key issue in the deposition technique is the injection of liquid. Low-density liquid has to penetrate the core of the jet in order for the heat treatment to result in a coating formation. Two major injection systems include atomization and continuous jet injection and are discussed elsewhere (Ref 5-10).

More recent studies use the continuous jet injection system instead. The suspension is introduced through a port inside the anode nozzle of a SG-100 plasma torch (Praxair S.T., Indianapolis, IN). The present study tests the influence of major operational process parameters, namely spray distance and electric power input to plasma on the microstructure of suspension plasma sprayed HA, starting from the parameters optimized previously (Ref 11). The microstructure investigations include x-ray diffraction (XRD) and energy-dispersive x-ray spectroscopy (EDS), which are routine techniques enabling identification of the phase content in sprayed HA coatings. The advanced techniques of microstructural investigation were transmission electron microscopy (TEM) and Raman microscopy. Transmission electron microscopy was used recently to characterize HA coatings plasma sprayed using nanostructured particles by Renghini et al. (Ref 12). This technique was also used to study the microstructure of suspension plasma sprayed TiO_2 by Podlesak et al. (Ref 13). Raman microscopy enables localization of the phases inside HA coating with a resolution of a few micrometers. An important advantage of this technique is the capability of identifying amorphous calcium phosphates (ACP) (Ref 14).

Harry Podlesak and **Thomas Lampke**, Chemnitz University of Technology, D-09107 Chemnitz, Germany; **Lech Pawlowski, Romain d'Haese,** and **Severine Bellayer**, Ecole Nationale Supérieure de Chimie de Lille, F-59652 Villeneuve d'Ascq, France; and **Jacky Laureyns**, University of Lille 1, F-59655 Villeneuve d'Ascq, France. Contact e-mail: lech.pawlowski@ensc-lille.fr.

2. Experimental

2.1 Suspension Preparation

The HA was synthesized using calcium nitrate and diammonium phosphate in ammonia solution according to:

$$6(NH_4)_2HPO_4 + 10Ca(NO_3)_2 + 8NH_4OH$$
$$\rightarrow 6H_2O + 20NH_4NO_3 + Ca_{10}(PO_4)_6(OH)_2 \quad (Eq\ 1)$$
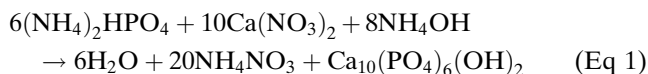
The detailed experimental procedure is described in a previous paper (Ref 15). The powder after calcination was crushed and ball milled using the MoliNex system (Netzsch, Germany) with 1.85 mm diameter zirconia balls and ethanol used as the cooling medium. The particle size distribution in ethanol is monomodal, and the mean diameter is about 1 μm. The XRD of initial powder reveals only hydroxyapatite without any other phase. The size distribution in water is bimodal, showing the formation of the agglomerates having size ranging from 3 to 10 μm. The suspension was formulated by taking about 20 wt.% of dry powder with 40 wt.% water and 40 wt.% ethanol.

2.2 Plasma Spray Parameters

The optimization of spray parameters was made with the use of substrates of titanium having size $20 \times 20 \times 0.8$ mm washed with ethanol and dried prior to the spraying. The corundum grit having granulometry of $-125 + 88$ μm was blasted under pressure of 0.4 MPa onto the substrates prior to coating deposition. The internal injection was made through a 0.5 mm internal diameter nozzle set in the port in the anode nozzle of the torch. The SG-100 torch (Praxair S.T., Indianapolis, IN) with anode 03083-175 and cathode 03083-129 and gas injector 03083-113, mounted on a five-axis ABB IRB-6 industrial robot (Zürich, Switzerland), was used throughout the experiments. The spray parameters, which were kept constant during the experiments, are collected in Table 1. The variable parameters were electric power input and spray distance. The experimental runs, which were designed with a help of 2^n design with one experiment in the center (Ref 16), are presented in Table 2. The coating surface temperature was recorded using a pyrometer IN 5 Plus (Impac, Erstein, France). The evolution of temperature for one of the experimental runs is shown in Fig. 1.

2.3 Microstructure Observations

2.3.1 X-Ray Diffraction. XRD investigations of sprayed coatings were done using Bruker apparatus type D8 (Karlsruhe, Germany) with Cu-Kα radiation in the range of 2θ angles from 20° to 60° with a low scan velocity of 2.6° (2θ angles)/h. The patterns were identified using Diffrac^{plus} Eva software (Bruker AXS, Karlsruhe, Germany), which is based on International Centre of Diffraction Data JCPDS-ICDD. The percentage of the other phases with regard to hydroxyapatite were determined from the reference intensity ratio (RIR), a method

Table 1 Constant parameters of suspension plasma spray

Spray parameters	Values
Plasma spray	
Electric power, kW	See Table 2
Working gases composition	$Ar + H_2$
Working gases flow rate, sLpm	45 + 5
Spray distance, mm	See Table 2
Number of scans	15; 3 series of 5 scans over substrate interrupted for about 1 min
Torch scan speed, mm/s	500
Suspension and injection	
Suspension feed rate, g/min	20
Injection	Internal through an internal port
Injector type	Nozzle with internal diameter of 0.5 mm
Geometry of internal injection	4 mm from jet axis; 16 mm backward from the anode-nozzle exit; right angle to jet axis
Static pressure in suspension container, MPa	0.05
Coating	
Thickness, μm	50-100
Coating surface temperature, °C	400-600, see also Fig. 1

Table 2 Variable parameters of suspension plasma spray

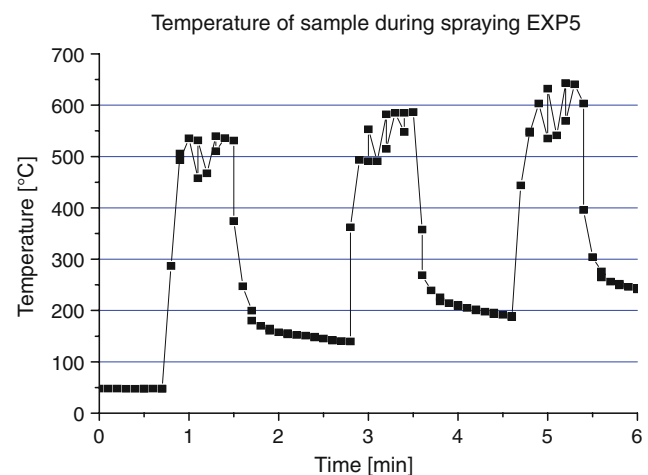| Run	Power input to plasma, kW	Spray distance, mm	Maximal temperature at spraying, °C
1	30	60	510
2	27	50	600
3	33	50	620
4	27	70	520
5	33	70	650

Fig. 1 Evolution of the coating surface temperature in experimental run No. 5

described by Prevey (Ref 17) using the comparison of strongest peak intensities. Reference intensity ratio values are calculated as I/I_c by software Diffrac^{plus} Eva, where I is

intensity of 100% peak of phase α and I_c is intensity of 100% peak of a 50/50 (by weight) mixture of this phase and corundum. Those values are read directly from the data sheets, and RIR factors are given in the PDF file of the JCPDS database:

- HA (hydroxyapatite), JCPDS 73-1731, $I/I_c = 1.1$
- α-TCP [tricalcium phosphate $Ca_3(PO_4)_2$], JCPDS 70-0374, $I/I_c = 0.5$
- β-TCP [tricalcium phosphate $Ca_3(PO_4)_2$], JCPDS 70-2065, $I/I_c = 1.3$
- TTCP (tetracalcium phosphate, $Ca_4P_2O_9$), JCPDS 70-1379, $I/I_c = 0.8$
- CaO (calcium oxide), JCPDS 82-1690, $I/I_c = 4.5$

2.3.2 Transmission Electron Microscopy. The specimens for TEM investigations were prepared as cross sections. The method of sample preparation was described previously (Ref 13). The TEM study used a Hitachi H8100 microscope (Hitachi, Japan) equipped with scanning unit and detector for secondary electrons at 200 kV with an energy-dispersive x-ray spectrometer EDAX Genesis XM2 (Ametek, NJ). Energy-dispersive spectrometric analysis of single grains was made with the diameter of the electron beam reduced to between 50 and 100 nm. Such elements as oxygen, phosphorus, and calcium were considered in the quantitative analysis. Because of the high uncertainty of the determination of the oxygen content, the ratio of atomic concentrations calcium to phosphorus was chosen to be examined. Additionally, the scanning electron microscopy (SEM) type Zeiss Neon40EsB (Zeiss, Jena, Germany) was used in the research.

2.3.3 EPMA. Microanalyses were carried out with a CAMECA SX100 (Cameca, Paris, France) electron probe microanalyzer. The backscattering electrons images and elemental analyses were made at 15 kV and 15 nA. TAP and PET crystals were used to detect, respectively, the Kα x-rays of the elements phosphorus and calcium. The profile of the chemical composition was made out with a step of 1 μm.

2.3.4 Raman Microscopy. The samples for Raman microscopy were embedded in epoxy resin (araldite) to observe the cross section of tested coatings. After the polymerization of the resin, the samples were mechanically ground and polished. Raman spectra were obtained by mean of a LabRAM Jobin-Yvon (Horiba Jobin Yvon, Tokyo, Japan) spectrometer, equipped with a computerized recording. Raman spectra were generated with the use of helium-neon (He-Ne) laser. The area analyzed with Raman microscope is about 1 μm². The spectra were initially collected for wavelengths ranging from 200 to 2000 cm^{-1}, and then the region from 400 to 1200 cm^{-1} was selected for further analyses. The samples were fluorescent under radiation, and the spectra should have been numerically treated.

3. Results

3.1 X-Ray Diffraction

The samples sprayed in different experimental runs contained HA as a major phase and the different phases of its decomposition in high temperature. The results of the phase analysis are shown in Table 3. The presence of the hydroxyapatite is the smallest, and the quantity of its decomposition phases is the greatest in the samples sprayed in experimental run No. 3. This run corresponded to the greatest electric power input and the shortest spray distance.

3.2 Transmission Electron Microscopy/ Electron-Dispersive Spectroscopy

A previous study made with use of SEM at the surface and on the cross section of layers shows the presence of two zones in the microstructure (Ref 11). The two zones, dense and sintered, are shown in Fig. 2. The TEM micrograph in Fig. 3 indicates that sintered zones contain small rounded crystals some hundred nm in size. This size might correspond roughly to the size of initial particles. The crystals contain phosphorus and calcium, and their atomic ratio corresponds to HA. The dense zone has a lamellar character, similar to that of coarse powder sprayed coatings. The combined TEM and EDS identified three areas in this zone in which the atomic ratio P/Ca and the size of crystals are different (Fig. 4 and Table 4):

- *Area A*, corresponding to HA grains of an equilateral shape and a size of a few hundred nm and the micropores
- *Area B*, characterized by a very high ratio of calcium/phosphorus (Ca/P), which may be attributed to the calcium phosphate rich in CaO having spherical nanometric grains

Table 3   Fraction of phases calculated from x-ray diagrams for the samples suspension plasma sprayed in different experimental runs

Crystal phase	Chemical composition	Phase content in different experimental runs, %				
		1	2	3	4	5
Hydroxyapatite	$Ca_5(PO_4)_3OH$	85.6	85.2	71.6	85.6	90.9
α-TCP	$Ca_3(PO_4)_2$	11.1	8.9	14.5	8.7	6.2
β-TCP		2.4	1.9	3.7	2.7	1.4
TTCP	$Ca_4P_2O_9$	0	3.6	9.4	1.7	0.1
CaO		0.8	0.4	0.8	1.2	1.4
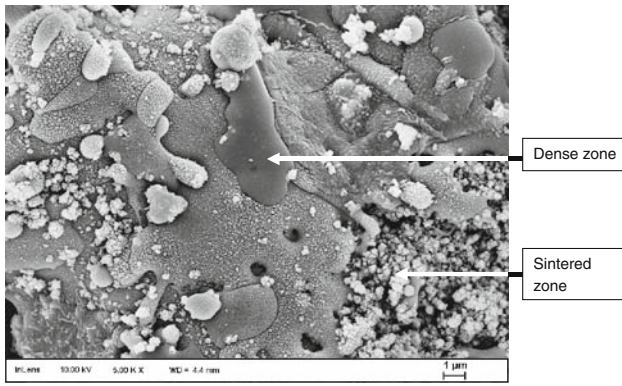
(a)
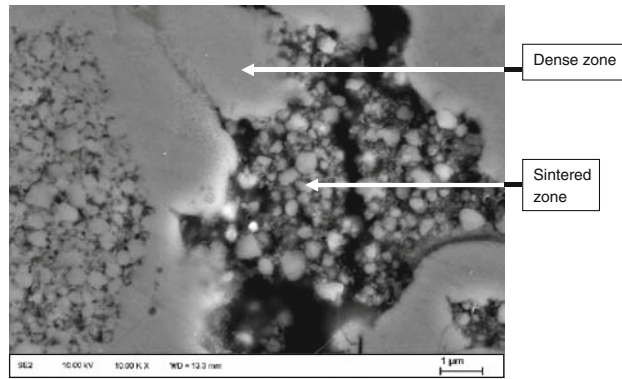
(b)

Fig. 2 Scanning electron micrographs of the coating sprayed in experimental run No.1. (a) Surface. (b) Cross section

- *Area C*, which corresponds to TTCP crystals of different shape and size.

3.3 Electron Probe Microanalysis

The microanalysis, made along the line crossing the coating section, shows the presence of the phases revealed already by TEM, namely, HA, TTCP, and CaO (Fig. 5). The strong variations of the chemical composition come from the porous sintered zone, which could have been impregnated with epoxy resin.

3.4 Raman Microscopy

The samples sprayed in experimental runs 2 and 5 were submitted to the Raman studies. The cross sections of the analyzed samples are shown in Fig. 6, and the corresponding spectra from the section areas close to the substrate and close to the surface are shown in Fig. 7. The broad peaks corresponding to the epoxy resin with the maxima at 830, 1150, and 1190 cm^{-1} are well visible on the areas close to the sample surface. The strong peak at 962 cm^{-1} corresponds to vibration mode ν_1 P-O of the tetrahedron PO_4^{-3} (Ref 18). The narrow peak is usually attributed to crystalline HA (Ref 19, 20). The shoulder of this peak at 952 cm^{-1} is attributed by these authors to amorphous calcium
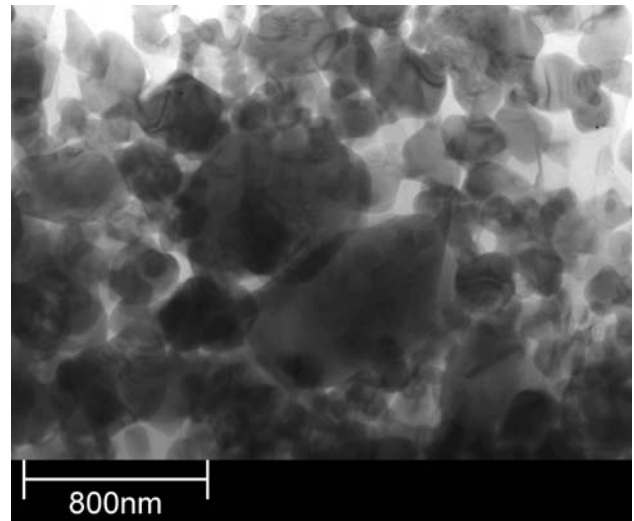
(a)
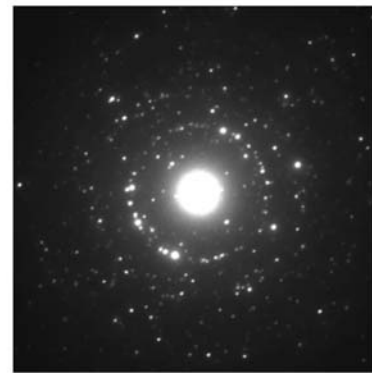
(b)

Fig. 3 Transmission electron micrographs of the sintered zone experimental in the sample sprayed in experimental run No. 1. (a) Bright field. (b) Selected area diffraction
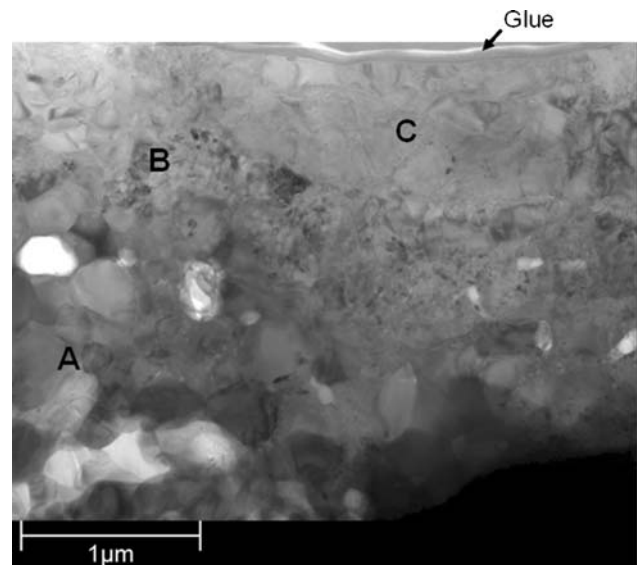

Fig. 4 Transmission electron micrographs of the dense zone in the sample sprayed in experimental run No. 1 with marked areas A, B, and C. The results of EDS study in the areas are given in Table 4

Table 4   Chemical composition and crystal size of the characteristic phases present in the dense zone (see also Fig. 4)

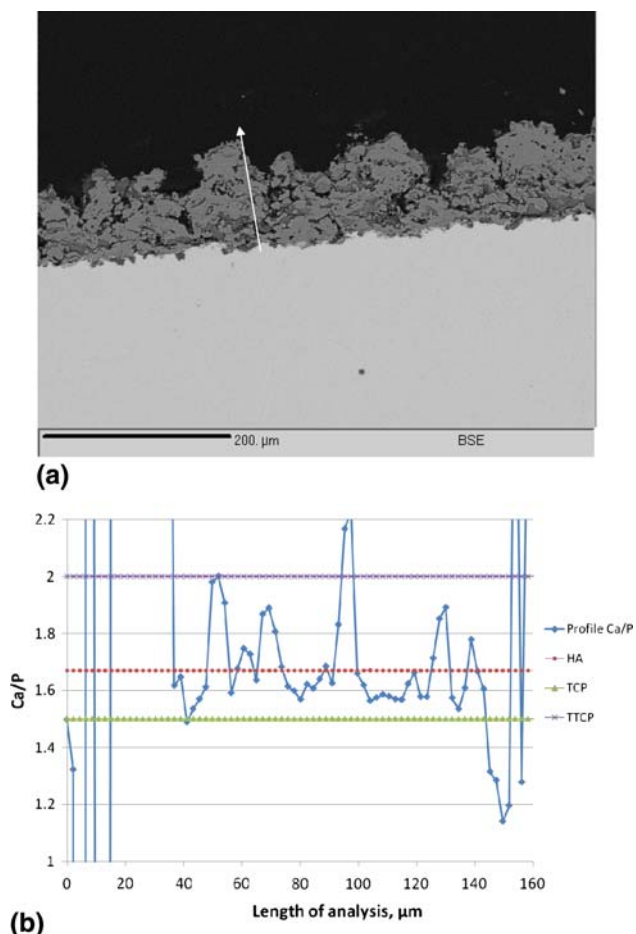|	Characteristic area		
	A	**B**	**C**
Ratio Ca/P found by EDS	1.70	About 4	About 2
Phase attributed	$Ca_5(PO_4)_3OH$	Calcium phosphate rich in CaO	$Ca_4P_2O_9$
Crystal size	Few hundreds of nm	Less than 50 nm	Very variable

Fig. 5 Electron microprobe analysis of a sample sprayed in experimental run No 2. (a) Scanning electron micrograph (backscattered electrons). (b) Ca/P ratio along the line

Fig. 6 Cross sections of samples submitted to Raman analysis and sprayed in experimental runs No. 2 (a) and No. 5 (b)

phosphates (ACP) or to TCP. Other peaks of the tetrahedron at 430 cm^{-1} corresponding to the O-P-O bending mode ν_2 and the bending mode at 596 cm^{-1} of the mode ν_4 were also observed and attributed to HA (Ref 14). The broad peaks at 615 to 650 cm^{-1} can be attributed to α- and β-TCP (Ref 20). The peaks are stronger at the interface with the substrate than at the coating surfaces.

4. Discussion

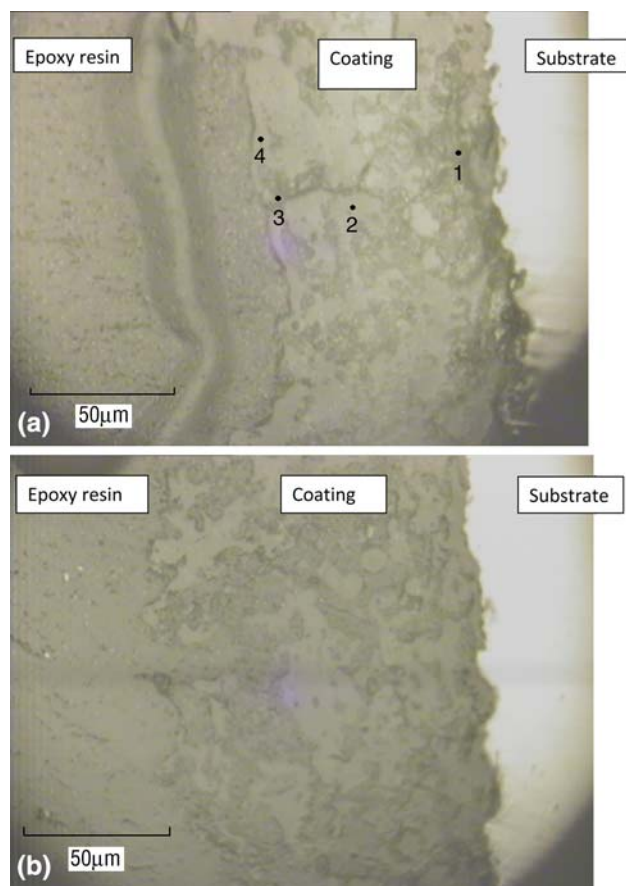Selected plasma sprayed parameters influence coating microstructure and in particular phase composition of the
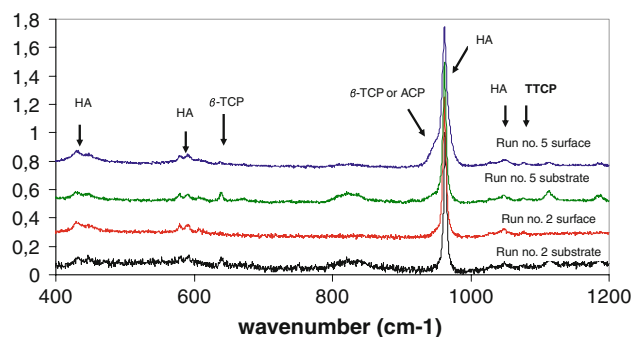

Fig. 7 Raman spectra of the regions close to the substrate and to the surface of the coatings shown in Fig. 6

coatings (see Table 3). The content of crystalline hydroxyapatite in the coatings has an important practical meaning and was analyzed more carefully. It seems that at the high power level of 33 kW, the spray distance strongly determines this content. At the low spray distance of 50 mm, the HA content was as low as 72% and increased up to 91% at the high-level spray distance of 70 mm (see Fig. 8). The effect of spray distance is related to the phenomena occurring at suspension plasma spraying. The phenomena, discussed in detail elsewhere (Ref 4, 11), include agglomeration of fine solids contained in the initial suspension in plasma jet. The agglomerates with a trajectory close to the jet centerline gets molten. The molten grains strike the substrate and deform, resulting in a well-known lamellar coating structure. Other agglomerates do not get molten and contribute in the sintered form to
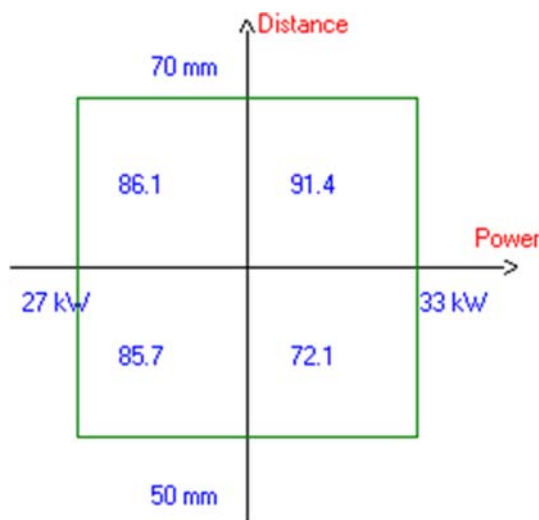

Fig. 8 Effects of spray variables on the content of hydroxyapatite in suspension plasma sprayed coatings

coating formation. The resulting, two-zone microstructure, is similar to that of the nanostructured coatings obtained from coarse feedstock that is agglomerated from fine particles by spray drying technique (see Fig. 2, 5a). The schematic representation of the technology of these two methods of coating manufacturing, shown in Fig. 9, makes it evident that suspension thermal spraying, which results in coatings having a microstructure shown in Fig. 9(a), saves one step in coating preparation, namely coarse powder agglomeration by spray drying or a similar technique. On the other hand, the microstructure similar to that shown in Fig. 9(b) was presented recently in WC-CoCr coatings sprayed by a high-velocity oxyfuel technique using powder agglomerated from submicrometric fine solids (Ref 21). The suspension plasma spraying makes it possible to agglomerate fine solids place directly in plasma jet. Some agglomerates get molten and contribute to the formation of dense zone of deposits, and the others remain loosely connected and form sintered zone. The discussion of each zone is made separately.

4.1 Dense Zone

The grains of the zone are composed of HA as the major phase and the phases of decompositions that are mainly TTCP and calcium phosphates rich in CaO. The formation of these phases can be interpreted by the condition of solidification of liquid particles arriving on the substrate. HA nucleated from calcium phosphate melt has the stoichiometric ratio of Ca/P = 1.67. The crystals of TTCP or calcium phosphate rich in CaO have the ratio of Ca/P $\geq$ 2. The presence of the different compounds inside a molten particle could have resulted from the selective evaporation of P_2O_5 from the particle surface in plasma jet (Ref 22, 23). The phase diagram predicts the formation of α-TCP that was not observed by TEM. The experimental observation should now be supported by a theoretical description of the nucleation of molten calcium phosphate
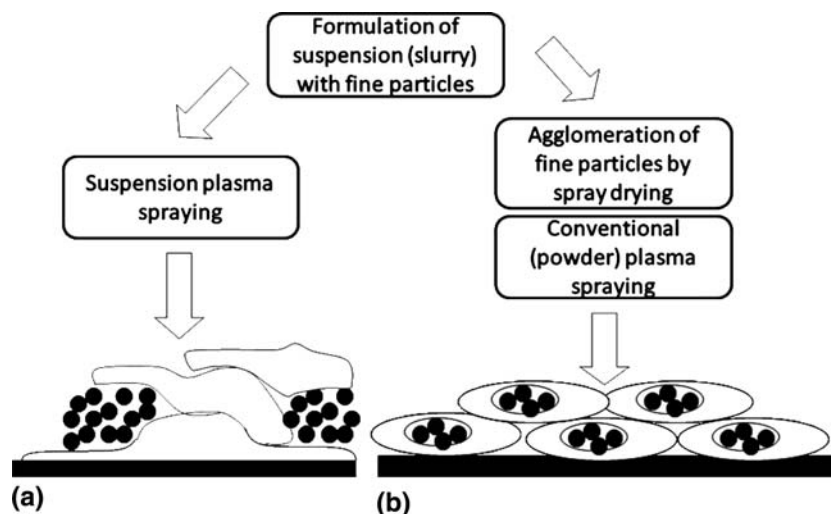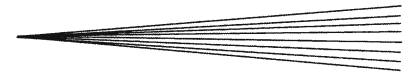

Fig. 9 Two routes leading to a formation of two-zone microstructure. (a) Suspension plasma spraying. (b) Agglomeration of coarse powders by spray drying followed by conventional plasma spraying

in the condition of suspension plasma spraying that includes rapid solidification and the strong convective heat input from the plasma jet.

4.2 Sintered Zone

The loosely agglomerated grains including initial HA fine particles arrive on the substrate. They get sintered during a flight in the periphery of the plasma jet, and the sintering process continues after deposition. This process is enhanced by the convective heat input from plasma being closer to the substrate compared with conventional spray process. This input results in high temperature at coating deposition demonstrated in Fig. 1. The analyses of entire coating cross sections, shown in Fig. 5 and 7, reveal that the phases are not distributed in the coatings in a homogeneous way.

5. Conclusions

Fine, home-synthesized, hydroxyapatite powder was formulated with water and alcohol to obtain a suspension used to plasma spray coatings onto the titanium substrate. The deposition process was optimized using statistical design of 2^n experiments with two variables: spray distance and electric power input to plasma. For a high power level of 33 kW, the phase composition was strongly dependent on the spray distance. X-ray diffraction was used to determine quantitatively the phase composition of obtained deposits. Raman microscopy and EPMA enabled localization of the phases in different position of the coating cross sections. Transmission electron microscopic study associated with energy-dispersive spectroscopy (EDS) enabled visualization and analysis of the two-zone microstructure. One zone contains crystals of hydroxyapatite, tetracalcium phosphate, and a phase rich in calcium oxide. The zone corresponds to the lamellas, usually observed in thermally sprayed coatings. The second zone contains fine hydroxyapatite grains that correspond to the fine nanometric and submicrometric solids from the suspension that were agglomerated and sintered in the cold regions of plasma jet and on the substrate. Further studies are needed to better explain the formation of the characteristic zones of the microstructure. Firstly, the conditions of nucleation of phases from a molten particle arriving on the substrate need to be clarified. Then the agglomeration and sintering of the fine submicrometric and nanometric solids in the plasma jet and by heat treatment during coating formation must be studied.

Acknowledgments

References

1. B.D. Ratner, A.S. Hoffman, F.J. Schoen, and J.E. Lemons, *Biomaterials Science: An Introduction to Materials in Medicine*, 2nd ed., Elsevier, Amsterdam, 2004, p 165
2. E. Bouyer, F. Gitzhofer, and M.I. Boulos, Suspension Plasma Spraying for Hydroxyapatite Powder Preparation by R.F. Plasma, *IEEE Trans. Plasma Sci.*, 1997, **25**(5), p 1066-1072
3. F. Gitzhofer, E. Bouyer, and M.I. Boulos, Suspension Plasma Spraying, U.S. Patent 5,609,921, November 3, 1997
4. L. Pawlowski, Suspension and Solution Thermal Spray Coatings, *Surf. Coat. Technol.*, 2009, **203**, p 2807-2829
5. R. Vaßen, H. Kaßner, G. Mauer, and D. Stöver, Suspension Plasma Spraying: Process Development and Applications, *ITSC 2009 Conference Proceedings*, CD ROM, ASM International, Materials Park, OH, 2009, ISBN 978-1-61503-004-0
6. R. Jaworski, L. Pawlowski, C. Pierlot, F. Roudet, S. Kozerski, and F. Petit, Suspension Plasma Sprayed Titanium Oxide and Hydroxyapatite Coatings, *ITSC 2009 Conference Proceedings*, CD ROM, ASM International, Materials Park, OH, 2009, ISBN 978-1-61503-004-0
7. F.-L. Toma, L.-M. Berger, C.C. Stahr, T. Naumann, and S. Langner, Microstructures and Functional Properties of Al_2O_3 and TiO_2 Suspension Sprayed Coatings: An Overview, *ITSC 2009 Conference Proceedings*, CD ROM, ASM International, Materials Park, OH, 2009, ISBN 978-1-61503-004-0
8. O. Tingaud, G. Montavon, A. Denoirjean, J.-F. Coudert, V. Rat, and P. Fauchais, Al_2O_3-ZrO_2 Finely Structured Multilayer Architectures from Suspension Plasma Spraying, *ITSC 2009 Conference Proceedings*, CD ROM, ASM International, Materials Park, OH, 2009, ISBN 978-1-61503-004-0
9. R. Jaworski, C. Pierlot, R. Tomaszek, L. Pawlowski, Z. Znamirowski, and J. Zdanowski, Optimization of Dielectric Properties of Suspension Plasma Sprayed Hydroxyapatite Coatings, *Materialwissen. Werkstofftechn.*, 2007, **38**(2), p 125-130
10. R. Tomaszek, L. Pawlowski, L. Gengembre, J. Laureyns, and A. Le Maguer, Microstructure of Suspension Plasma Sprayed Multilayer Coatings of Hydroxyapatite and Titanium Oxide, *Surf. Coat. Technol.*, 2007, **201**(16-17), p 7432-7440
11. S. Kozerski, L. Pawlowski, R. Jaworski, F. Roudet, and F. Roudet, Two Zones Microstructure of Suspension Plasma Sprayed Hydroxyapatite Coatings, *Surf. Coat. Technol.*, 2010, **204**(9-10), p 1380-1387
12. C. Renghini, E. Girardin, A.S. Fomin, A. Manescu, A. Sabbioni, S.M. Barinov, V.S. Komlev, G. Albertini, and F. Fiori, Plasma Sprayed Hydroxyapatite Coatings from Nanostructured Granules, *Mater. Sci. Eng. B*, 2008, **152**(1-3), p 86-90
13. H. Podlesak, L. Pawlowski, J. Laureyns, R. Jaworski, and T. Lampke, Advanced Microstructural Study of Suspension Plasma Sprayed Titanium Oxide Coatings, *Surf. Coat. Technol.*, 2008, **202**(15), p 3723-3731
14. R.B. Heimann, Novel Approaches Towards Design and Biofunctionality of Plasma-Sprayed Osteoconductive Calcium Phosphate Coatings for Biomedical Implants: The Concept of Bond Coats, *Trends in Biomaterial Research*, P.J. Pannone, Ed., Nova Publishers, NY, 2007, p 1-80, ISBN 1-978-1-60021-361-8
15. R. Jaworski, C. Pierlot, L. Pawlowski, M. Bigan, and M. Martel, Synthesis and Preliminary Tests of Suspension Plasma Spraying of fine Hydroxyapatite Powder, *J. Thermal Spray Technol.*, 2008, **17**(5-6), p 679-684
16. C. Pierlot, L. Pawlowski, M. Bigan, and P. Chagnon, Design of Experiments in Thermal Spraying: A Review, *Surf. Coat. Technol.*, 2008, **202**(18), p 4483-4489
17. P.S. Prevey, X-Ray Diffraction of Crystallinity and Phase Composition in Plasma Sprayed Hydroxyapatite Coatings, *J. Thermal Spray Technol.*, 2000, **9**(3), p 369-376
18. L. Yan, Y. Leng, and L.-T. Weng, Characterization of Chemical Inhomogeneity in Plasma-Sprayed Hydroxyapatite Coatings, *Biomaterials*, 2003, **24**, p 2585-2592
19. K.A. Gross and M.R. Phillips, Identification and Mapping of the Amorphous Phase in Plasma-Sprayed Hydroxyapatite Coatings

Using Scanning Cathodoluminescence Microscopy, *J. Mater. Sci. Mater. Med.*, 1998, **9**, p 797-802

20. H. Li, B.S. Ng, K.A. Khor, P. Cheang, and T.W. Clyne, Raman Spectroscopy Determination of Phases Within Thermal Sprayed Hydroxyapatite Splats and Subsequent In Vitro Dissolution Examination, *Acta Mater.*, 2004, **52**, p 445-453

21. A. Ghabchi, T. Varis, E. Turunen, T. Suhonen, X. Liu, and S.-P. Hannula, Behavior of HVOF WC-10Co4Cr Coatings with Different Carbide Size in Fine and Coarse Particle Abrasion, *ITSC 2009 Conference Proceedings*, CD ROM, ASM International, Materials Park, OH, 2009, ISBN 978-1-61503-004-0

22. S. Dyshlovenko, B. Pateyron, L. Pawlowski, and D. Murano, Numerical Simulations of Hydroxyapatite Powder Behaviour in Plasma Jet, *Surf. Coat. Technol.*, 2004, **179**(1), p 110-117

23. S. Dyshlovenko, L. Pawlowski, B. Pateyron, I. Smurov, and J.H. Harding, Modelling of Plasma Particles Interactions and Coating Growth for Plasma Spraying of Hydroxyapatite, *Surf. Coat. Technol.*, 2006, **200**, p 3757-3769